[C-11]PIB PET imaging can detect white and grey matter demyelination in a non-human primate model of progressive multiple sclerosis

Carvalho, Robert H. F.; Real, Caroline C.; Cinini, Simone; Garcez, Alexandre T.; Duran, Fabio L. S.; Marques, Fabio L. N.; Mello, Luiz Eugenio; Busatto Filho, Geraldo; de Vries, Erik F. J.; de Britto, Luiz R. G.

Published in:
Multiple Sclerosis and Related Disorders

DOI:
10.1016/j.msard.2019.07.020

Publication date:
2019

[^{11}C]PIB PET imaging can detect white and grey matter demyelination in a non-human primate model of progressive multiple sclerosis

Robert H.F. Carvalho[#a], Caroline C. Real[#a], Simone Cinini[b], Alexandre T. Garcez[a], Fabio L.S. Duran[c], Fabio L.N. Marques[a], Luiz Eugênio Mello[b], Geraldo Busatto Filho[c], Erik F.J. de Vries[d], Luiz R.G. de Britto[e], Carlos A. Buchpiguel[a], Daniele de Paula Faria*[a]

a) Laboratory of Nuclear Medicine (LIM-43), Departamento de Radiologia e Oncologia, Faculdade de Medicina, Universidade de Sao Paulo, Sao Paulo, SP, BR.
b) Department of Physiology, Escola Paulista de Medicina, Universidade Federal de Sao Paulo, Sao Paulo, SP, BR.
c) Laboratory of Psychiatric Neuroimaging (LIM-21), Departamento de Psiquiatria, Faculdade de Medicina, Universidade de Sao Paulo, Sao Paulo, SP, BR.
d) Department of Nuclear Medicine and Molecular Imaging, University Medical Center Groningen, University of Groningen, Groningen, The Netherlands.
e) Laboratory of Cellular Neurobiology, Departamento de Fisiologia e Biofísica, Universidade de Sao Paulo, Sao Paulo, SP, BR.

***Corresponding author:**

Daniele de Paula Faria

danielefaria1@gmail.com

Center of Nuclear Medicine building, 2nd floor

Rua Doutor Ovidio Pires de Campos, 872, Cerqueira Cesar, São Paulo/SP, Brazil

Zip code: 05403-911

Phone: +55 11 26618053

 # Robert H. F. Carvalho and Caroline C. Real have contributed equally to the work.

Running title: Demyelination detection by ^{11}C-PIB PET

Abstract

Background: Multiple sclerosis (MS) is a demyelinating and inflammatory disease of the central nervous system. Its diagnosis is clinical, often confirmed by magnetic resonance imaging. This image modality, however, is not ideal for discrimination of demyelination in grey and white matter regions from inflammatory lesions. Positron Emission Tomography (PET), using specific radiopharmaceuticals, can be a tool to differentiate between these processes. The radiopharmaceutical [^{11}C]PIB is widely used for detection of β-amyloid plaques, but has also been suggested for the analysis of myelin content due to its consistent uptake in white matter. The aim of this study was to evaluate [^{11}C]PIB PET imaging as a tool for detecting demyelinated regions in white and grey matter of non-human primate model of progressive MS. **Methods:** Experimental autoimmune encephalomyelitis (EAE) was induced in marmosets by injection of recombinant human myelin oligodendrocyte glycoprotein (rhMOG) emulsified in either Incomplete Freund's Adjuvant (IFA) or Complete Freund's Adjuvant (CFA). [^{11}C]PIB PET images were acquired prior to immunization (baseline) and after symptoms were present (end of experiment). Brain tissue was isolated for histochemical analysis. **Results:** All rhMOG/IFA-treated and rhMOG/CFA-treated animals showed clinical signs of EAE. The rhMOG/CFA group presented a significant [^{11}C]PIB uptake reduction only in the left motor cortex (9 %, P = 0.011). For the rhMOG/IFA group, significant decrease in [^{11}C]PIB uptake was observed in the whole brain (15 %, P = 0.015), in the right hemisphere of body of corpus callosum (34 %, P = 0.02), splenium of corpus callosum (38 %, P = 0.004), hippocampus (19%, P = 0.036), optic tract (13 %, P = 0.025), thalamus (14 %, P = 0.041), Globus pallidus (23 %, P = 0.017), head of caudate nucleus (25 %, P = 0.045), tail of caudate nucleus (29 %, P = 0.003), putamen (28 %, P = 0.047) and left hemisphere of body of corpus callosum (14 %, P = 0.037) and head of caudate nucleus (23 %, P = 0.023). [^{11}C]PIB uptake significantly correlated with luxol fast blue histology (myelin marker), both in the rhMOG/IFA (r^2= 0.32, P < 0.0001) and the rhMOG/CFA group (r^2= 0.46, P < 0.0001). **Conclusion:** [^{11}C]PIB PET imaging is an efficient tool for detecting demyelination in grey and white matter, in a non-human primate model of progressive MS.

Keywords: Multiple sclerosis; EAE marmoset model; PET imaging; Pittsburgh compound B

Introduction

Multiple sclerosis (MS) is a demyelinating and inflammatory disease of the central nervous system (CNS) *(1)*. MS can present as different phenotypes: 1) Relapsing-remitting multiple sclerosis, characterized by periods of attacks and recovery and 2) Progressive multiple sclerosis which is characterized by worsening of disability that can be present either from disease onset (Primary Progressive) or after a relapsing-remitting course (Secondary Progressive) *(2)*. The pathological feature of multiple sclerosis is the formation of multiple focal demyelinated areas in the CNS, both in white and grey matter *(3)*.

Studies with animal models have been helpful to increase our understanding of the human disease *(4)*. The experimental autoimmune encephalomyelitis model (EAE) presents MS-like features in brain and spinal cord, including white and grey matter lesions *(5)*. Although the EAE model can be induced in several animal species, the common marmoset (*Callithrix jacchus*) EAE model has emerged as the most suitable animal model of progressive MS, because it closely mimic the MS disease characteristics in humans. The most widely used methods to induce EAE are an intradermal injection of recombinant human myelin oligodendrocyte glycoprotein (rhMOG-125) or synthetic human myelin oligodendrocyte glycoprotein peptide for amino acids 34-56 (MOG 34-56) in combination with incomplete Freund's adjuvant (IFA) or complete Freund's adjuvant (CFA) *(6)*, although immunization with rhMOG-125 more closely mimics autoimmune development in MS patients *(7)*.

Non-invasive *in vivo* imaging tools are also of great relevance in MS. Magnetic resonance imaging (MRI) is the most frequently used imaging modality for MS diagnosis and monitoring of disease progression. However, this modality has limitations in differentiating between inflammation, axon loss, demyelination and remyelination *(8)*. Positron emission tomography (PET) is an imaging modality able to detect changes at the cellular and molecular level and may be able to differentiate between inflammation, myelin content, and neurodegeneration, using process-specific PET tracers. The first human myelin PET imaging

study in patients was performed in 2011*(9)*, using [^{11}C]PIB as a PET tracer, and after that, studies in rodent animal models were performed *(10-12)*. [^{11}C]PIB has been widely used for imaging β-amyloid plaques in Alzheimer´s disease, but its high binding to white matter, independent of the presence of β-amyloid plaques *(13)*, led to the investigation of its potential as a myelin PET tracer *(9)*.

Considering that [^{11}C]PIB PET could be an useful tool for quantifying myelin content, this study aimed to evaluate the feasibility of detecting demyelination in both grey and white matter in non-human primate model of progressive multiple sclerosis.

Materials and Methods

Animals

All experiments with marmosets were approved by the Ethical Committee of the Federal University of São Paulo (UNIFESP 2628300415) and Faculty of Medicine of the University of São Paulo (FMUSP 056/15). The *Callithrix jacchus*, popularly known as marmosets (n = 10, 7 females and 3 males) were provided by the Neurophysiology Laboratory of UNIFESP. Animals were kept alone in spacious cages enriched with branches and ropes in a temperature and humidity controlled room with a 12h-light cycle. Animals were fed in the morning with 5 types of fruit, and in the afternoon with vegetables and proteins, water was available *ad libitum.* The animals were kept in the primate facility throughout the experimental period and transported to the nuclear medicine laboratory only for PET image acquisitions. The transport of the animals was authorized by The Secretariat for the Environment of the State of São Paulo (SMA - SP).

Marmosets were divided into two groups (n = 5), according to the immunization protocol, using either rhMOG/IFA emulsion or rhMOG/CFA emulsion as the immunizing agent.

Experimental autoimmune encephalomyelitis induction

The EAE model was induced as previously reported *(7, 14, 15)*. The emulsions for EAE induction consisted of 100 μg rhMOG dissolved in 200 μL of PBS and emulsified in 200 μL of either IFA (Becton, Dickinson and Company, BD263910) or CFA (Sigma-Aldrich, F5881). In anesthetized animals (3% isoflurane in oxygen) the emulsion (100 μL) were intradermally inoculated into 4 sites of inguinal and axillary regions of dorsal skin (400 μL emulsion injected per animal).

The marmosets were evaluated daily for neurological signs *(15)*: 0 = no clinical signs; 0.5 = apathy, loss of appetite, altered walking pattern without ataxia; 1 = lethargy, anorexia, loss of tail tonus, tremor; 2 = ataxia, optic disease; 2.5 = paraparesis or monoparesis, sensory loss; 3 = paraplegia or hemiplegia; 4 = quadriplegia; 5 = spontaneous death due to EAE *(15)*. If no clinical symptoms were detected until 4 weeks after immunization, the animal received a booster-immunization, which was repeated every 4 weeks until symptoms appeared. Body weight was checked twice a week.

[^{11}C]PIB production and PET imaging

[^{11}C]PIB was produced at Nuclear Medicine Center, FMUSP, with a radiochemical purity > 95% and a molar activity > 20 GBq/μmol.

[^{11}C]PIB PET was performed at two different time points: baseline (i.e. before EAE induction) and after clinical symptoms had appeared. The definition of the second time point was based on reaching one of the following criteria: 1) Score 3; 2) Score 2 – 2.5 and 10% body weight loss; 3) Score 1 - 2 and persistent body weight loss (more than 10 days) and 4) Body weight loss ≥ 20%.

The marmosets were anesthetized with isoflurane mixed with oxygen and then injected in the femoral or penile vein with 37-111 MBq of [^{11}C]PIB. Thirty minutes after injection, animals were positioned with their head in the center of the field of view of a small-animal PET

scanner (Triumph™ - Gamma Medica-Ideas, Northridge, CA, U.S.A). A static image was acquired for 30 min. The body temperature of the animals was maintained by heating pads and breath rate were monitored. After the scans, the animals were either allowed to recover in their home cages (baseline) or euthanized (end of experiment) with 1 mL of intraperitoneal pentobarbital (0.3 mg/mL). The brain was dissected for myelin histochemistry.

PET image reconstruction and analysis

Emission sinograms were iteratively reconstructed into a single frame of 30 min (OSEM 3D; 20 iterations and 4 subsets), after being normalized and corrected for attenuation, scatter, and radioactivity decay. PET image analysis was performed with PMOD 3.4 software (PMOD™ Technologies Ltd, Switzerland). The scans were manually co-registered to a T2 weighted MRI template (http://brainatlas.brain.riken.jp/marmoset/modules/xoonips/listitem.php?index_id=71) to facilitate the identification of different brain regions.

Volumes of interest (VOIs) for 39 brain regions were drawn on the MRI template based on the marmoset brain atlas *(16).* An extracellular VOI of a nonspecific [^{11}C]PIB binding area was also drawn, being the muscle attached to the skull selected as reference region *(17)* since no demyelination would occur in this area, meaning that this region, also present in the FOV, would not be affected by disease stage, clinical symptoms or booster-immunization; which cannot be guaranteed by the regions inside the brain, since all regions could present lesion in some stage. A reference region was necessary for the quantification due to the fact that some tracer injections were not perfectly performed (difficulties in vein punction of the marmoset) and the amount of injected activity injected could not accurately be determined.

The tracer uptake is presented as brain VOI-to-muscle VOI uptake ratio.

***In vitro* assays**

[^{11}C]PIB uptake in the brain was also analyzed by *in vitro* autoradiography as previously described *(18)*. Dried sections were exposed to a high resolution phosphor storage screen for 2 h and then, scanned by a Typhoon FLA 9500 biomolecular imager (GE Healthcare).

The level of myelin in different brain areas was assessed by luxol fast blue (LFB) histochemistry as previously described *(19)*. In each brain region (covering the whole brain – 20 to 30 samples per animal), areas with lesion and non-lesion were drawn and the integrated density ratio was calculated by Image J software (NIH/USA). In case no lesion was identified, the ratio was calculated by drawing two normal areas in the same brain region.

Statistical analysis

Results are presented as mean ± standard error (SPSS Statistics 20 Software, Armonk, NY: IBM Corp, USA and GraphPad Prism 6 Software, La Jolla, CA, USA)**.** The data (animal model, PET imaging and *in vitro* assays) passed the Shapiro-Wilk test for normality and therefore parametric tests were applied in the analysis. The PET imaging data was analyzed by a 3-way mixed ANOVA with repeated measures (considering groups as between and time and VOIs as within-subject factors). Post-hoc paired t-test (Bonferroni) with multiple comparison correction was performed to test tracer uptake differences between the baseline and end of experiment scan for each VOI. An unpaired *Student's t-test* was used for comparing the groups in the end of experiment time point (clinical symptoms, number of immunizations and body weight loss). Pearson correlation was used in the correlation between histological and in vivo PET imaging ([^{11}C]PIB uptake) results. P values < 0.05 were considered statistically significant.

Results

EAE disease progression

At the start of the experiment, the rhMOG/IFA and rhMOG/CFA group consisted of 5 animals each, but 1 animal was excluded from each group. In the rhMOG/IFA group, animal M4 was excluded due to unexplained death 2 days after the baseline PET scan. In the rhMOG/CFA group, animal M9 was excluded because it died during the end of experiment PET acquisition (possibly associated to anesthesia). For the remaining animals, the EAE symptoms was 100% for both immunization methods.

In general, immunization with rhMOG/IFA resulted in a less aggressive EAE model, as the first clinical symptoms started to appear later (101 ± 6 vs. 74 ± 18 days after the first immunization, P = 0.21) and more booster immunizations (2.75 ± 0.25 vs. 1.50 ± 0.50, P = 0.066) were necessary, when compared to immunization with rhMOG/CFA. Body weight loss at the end of the experiment was significantly less after immunization with rhMOG/IFA than with rhMOG/CFA (9.2 ± 2.0% vs.17.4 ± 2.3%, P = 0.028), as is illustrated in figure 1.

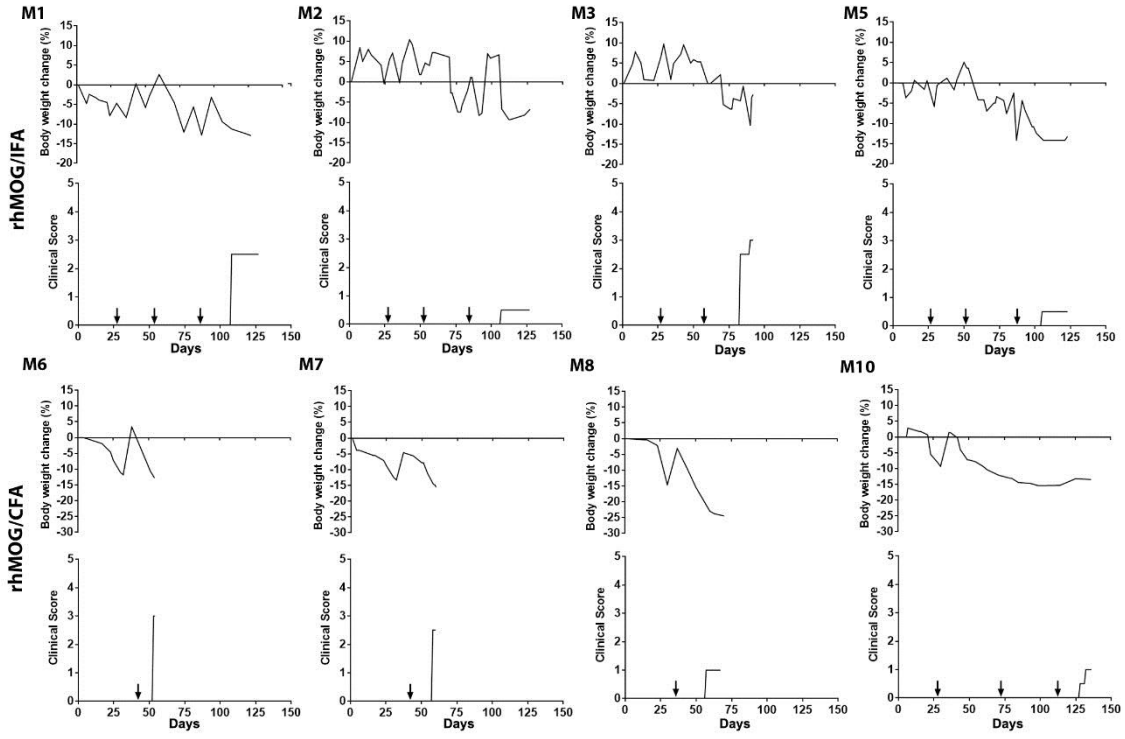

FIGURE 1. Body weight changes and clinical scores of rhMOG/IFA and rhMOG/CFA induced EAE. Marmosets immunized with rhMOG/IFA (top) and with rhMOG/CFA (bottom). Arrows indicate booster immunizations, which happened every 4 weeks in animals without overt signs of EAE.

PET imaging of demyelination

Representative [^{11}C]PIB PET images are illustrated in figure 2. Statistical analysis revealed a main effect for time [F(1,6) = 16.556; P = 0.007] and VOIs [F(38,228) = 7.489; P = 0.0001], but not for group [F(1,6) = 2.143; P = 0.194]. There were an interaction between VOIs and groups [F(38,228) = 1.657; P = 0.013], but not for time and groups [F(1,6) = 1.987; P = 0.208], VOIs and time [F(38,228) = 1.086; P = 0.346], and VOIs, time and groups [F(38,228) = 0.919; P = 0.610]. Multivariate test revealed a significant time effect on rhMOG/IFA group F(1,6) = 15.007; P=0.008], but not on rhMOG/CFA group [F(1,6) = 3.536; P=0.109].

In the rhMOG/IFA group, the [^{11}C]PIB uptake ratio was significantly reduced at the end of the study, when compared to baseline in the whole brain (1.48 ± 0.03 vs. 1.25 ± 0.08, P = 0.015), right body of corpus callosum (1.62 ± 0.05 vs. 1.07 ± 0.25, P = 0.024), right splenium of corpus callosum (1.72 ± 0.04 vs. 1.06 ± 0.22, P = 0.004), right hippocampus (1.49 ± 0.05 vs. 1.21 ± 0.08, P = 0.036), right optic tract (1.56 ± 0.05 vs. 1.36 ± 0.10, P = 0.025), right thalamus (1.55 ± 0.04 vs. 1.33 ± 0.11, P = 0.041), right Globus pallidus (1.75 ± 0.08 vs. 1.35 ± 0.16, P = 0.017), right head of caudate nucleus (1.55 ± 0.09 vs. 1.67 ± 0.20, P = 0.045), right tail of caudate nucleus (1.76 ± 0.11 vs. 1.24 ± 0.15, P = 0.003), right putamen (1.66 ± 0.06 vs. 1.20 ± 0.25, P = 0.047), left body of corpus callosum (1.58 ± 0.08 vs. 1.36 ± 0.04, P = 0.037) and left head of caudate nucleus (1.69 ± 0.05 vs. 1.30 ± 0.11, P = 0.023). In the rhMOG/CFA group a significant decreased [^{11}C]PIB uptake ratio was observed in the motor cortex in the left hemisphere (1.37 ± 0.05 vs. 1.24 ± 0.03, P = 0.011).

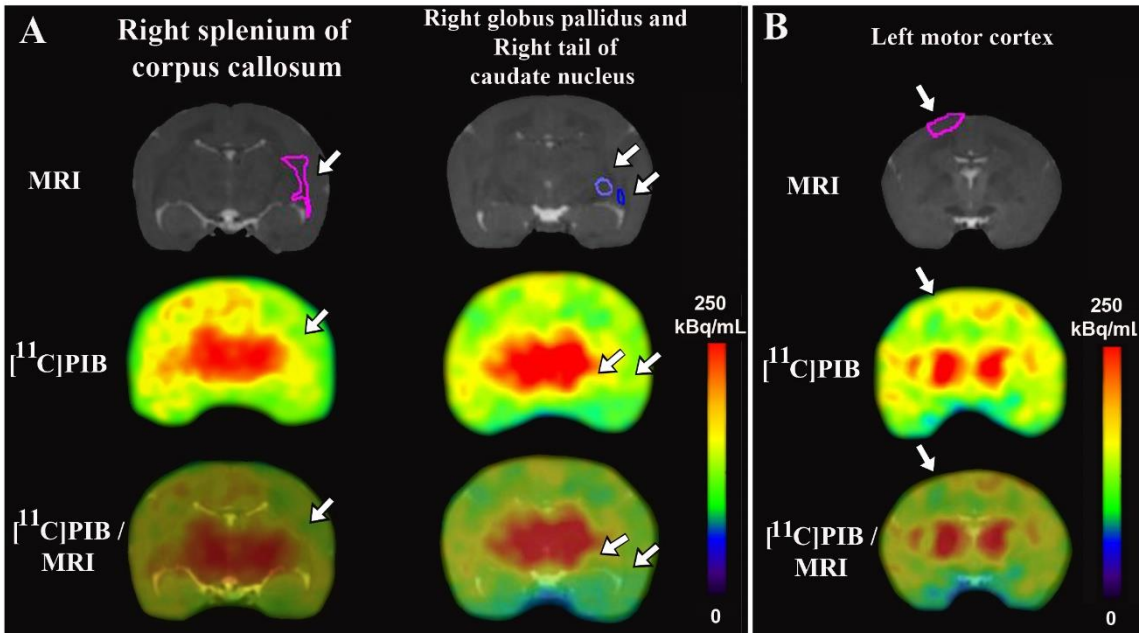

FIGURE 2. [^{11}C]PIB PET illustrative images of the end of experiment scans showing different regions of significantly decreased tracer uptake. VOIs for quantification were drawn on a MRI template (upper row). Middle row, [^{11}C]PIB PET images. Bottom row, [^{11}C]PIB PET images fused with the MRI template. A) rhMOG/IFA group and B) rhMOG/CFA group.

Although only some regions were statically significant in group comparisons it was possible to observe clear [^{11}C]PIB uptake differences in several areas of the brain when looking individually to the animals (Figure 3 and Tables 1 and 2).

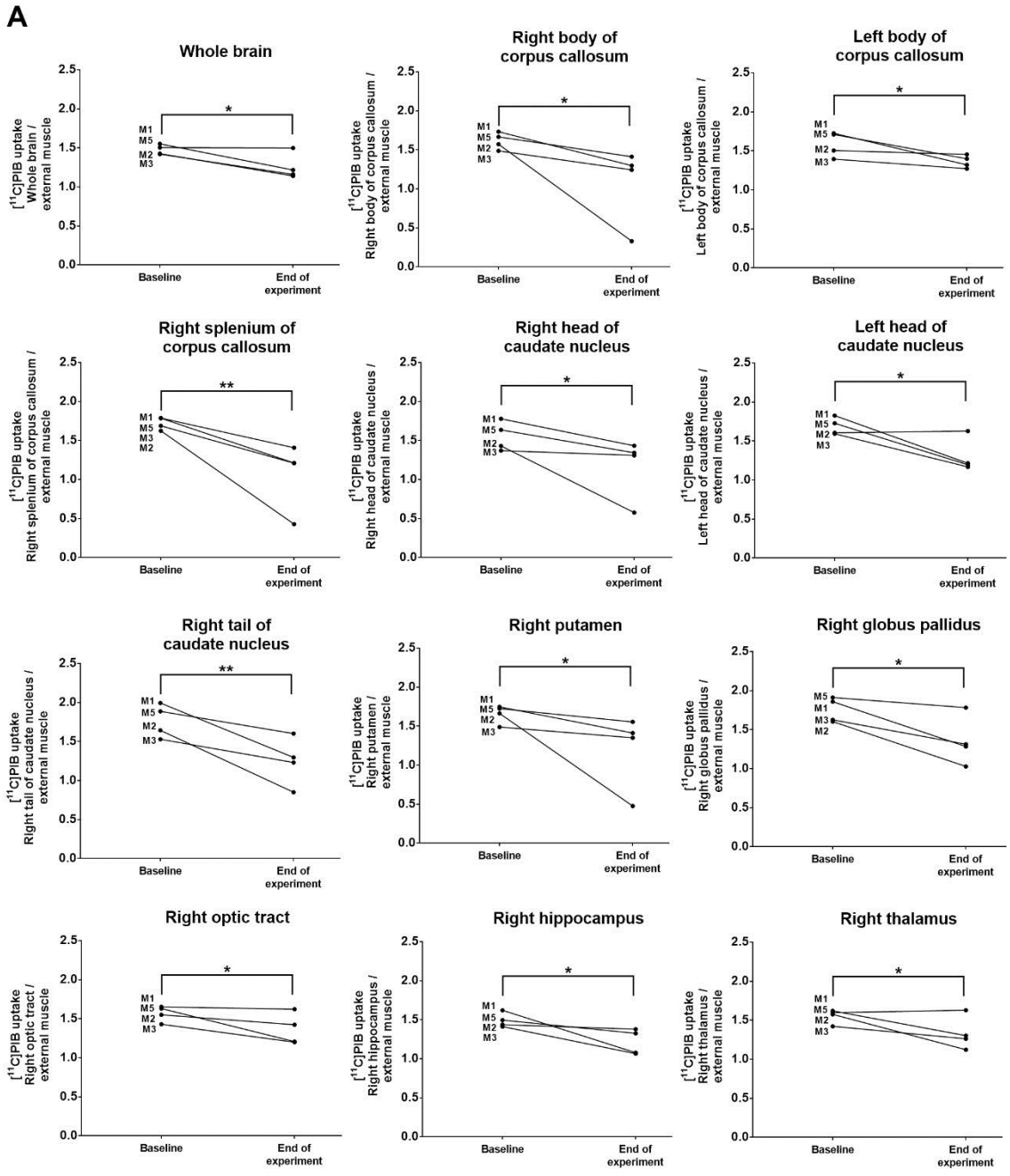
A
Whole brain
Right body of corpus callosum
Left body of corpus callosum
Right splenium of corpus callosum
Right head of caudate nucleus
Left head of caudate nucleus
Right tail of caudate nucleus
Right putamen
Right globus pallidus
Right optic tract
Right hippocampus
Right thalamus
[11C]PIB uptake
Baseline
End of experiment
B
Left motor cortex

FIGURE 3. [^{11}C]PIB PET uptake ratio of the baseline and end of the experiment scans in different brain areas of rhMOG/IFA group (A) and rhMOG/CFA group. Each graph represents one region with its respective name on the top. *P < 0.05, **P < 0.01.

TABLE 1: [^{11}C]PIB uptake differences, presented as percentage, between baseline and end of experiment in the different brain areas of each animal of the rhMOG/IFA group. Arrows indicate either decreased uptake (↓) or increased uptake (↑). Bold numbers indicate differences > 25%.

	IFA							
Volume of Interest (Antero-posterior coordinates relative to Bregma *(16)*)	**M1 (%)**		**M2 (%)**		**M3 (%)**		**M5 (%)**	
Whole brain (12.1 → - 8.9)	↓21		↓20		↓18		0	
Brainstem (- 2.9 → - 6.9)	↓21		**↓28**		↓21		↑11	
Cerebellum (- 6.2 → - 10.9)	↓15		↓20		**↓25**		↑18	
	Right	**Left**	**Right**	**Left**	**Right**	**Left**	**Right**	**Left**
Anterior commissure (6.6→ 5.6)	↑4	↓22	↓14	↑8	↑8	↓22	0	↓11
Body of corpus callosum (10.7→ - 6.9)	**↓25**	↓24	**↓79**	↓3	↓16	↓9	↓15	↓18
Cingulate cortex (10.7 → 4.9)	↓11	↓8	**↓60**	**↓36**	↓24	**↓26**	↑5	↑8
Globus pallidus (4.1→ 1.4)	**↓31**	↓17	**↓36**	**↑25**	↓19	↓4	↓7	↓7
Head of caudate nucleus (8.4→ 1.1)	↓19	**↓34**	**↓60**	↑1	↓4	**↓27**	↓18	**↓31**
Hippocampus (2.7→ - 3.2)	**↓33**	↓24	↓4	↑23	**↓25**	↓12	↓11	↓6
Internal capsule (9.4→ 1.1)	↓12	↓21	**↓53**	↑10	↑10	↓18	↓13	↓16
Midbrain (0.4→ - 4.4)	**↓25**	↓24	↓13	↑9	**↓26**	↓20	↑17	↑15
Motor cortex (10.4 → 4.9)	↓2	↓11	**↓83**	↓10	↓12	↑2	↑4	↑1
Optic tract (6.6→ 1.7)	**↓26**	**↓30**	↓8	↑10	↓16	**↓31**	↓2	↑8
Primary somatosensory cortex (4.9→ 4.4)	↓15	↓6	**↓88**	↓17	↓10	↑5	↓6	↑2
Putamen (8.4→ 1.4)	↓19	↓17	**↓71**	↓14	↓9	↑12	↓10	↓9
Somatosensory association cortex (4.1→ 1.1)	↓4	↓12	**↓87**	↑23	↓20	**↓26**	↓4	↓21
Splenium of corpus callosum (4.4→ - 3.2)	**↓32**	↓24	**↓74**	**↑35**	**↓28**	↓10	↓21	↓20
Subpial cortex (12.1→ - 8.6)	↓13	↓6	**↓68**	**↑27**	↓13	↓12	↑6	↓2
Tail of caudate nucleus (3.3→ 1.4)	**↓35**	**↓34**	**↓48**	↑21	↓20	**↓29**	↓15	↓11
Thalamus (3.3→ 0.7)	↓20	**↓28**	**↓29**	↑17	↓11	↓12	↑2	↑8
Visual cortex (- 6.2→ - 10.9)	**↓28**	**↓32**	**↓68**	↑23	**↓29**	↓20	↑12	↑14

Table 2: [^{11}C]PIB uptake differences, presented as percentage, between baseline and end of experiment in the different brain areas of each animal of the rhMOG/CFA group. Arrows indicate either decreased uptake (↓) or increased uptake (↑). Bold numbers indicate differences > 25%.

	CFA							
Volume of Interest (Antero-posterior coordinates relative to Bregma *(16)*)	**M6 (%)**		**M7 (%)**		**M8 (%)**		**M10 (%)**	
Whole brain (12.1→ - 8.9)	↓10		↓10		↑3		↓17	
Brainstem (- 2.9→ - 6.9)	↓8		↓9		↓1		↓14	
Cerebellum (- 6.2→ - 10.9)	↓3		↓12		↓3		↓18	
	Right	**Left**	**Right**	**Left**	**Right**	**Left**	**Right**	**Left**
Anterior commissure (6.6→ 5.6)	↓15	↓12	↓11	↓8	↓3	↑13	↓6	↑1
Body of corpus callosum (10.7→ - 6.9)	↓21	↓16	↓9	↓18	↑7	↑6	↓18	↑17
Cingulate córtex (10.7→ 4.9)	↓16	↓10	↓2	↓10	↓3	0	↓24	↓6
Globus pallidus (4.1→ 1.4)	↓19	↓10	↓3	↓16	↑12	↑13	↓23	↓14
Head of caudate nucleus (8.4 → 1.1)	**↓28**	↓17	↓9	↓11	↑15	↑20	↓15	↓4
Hippocampus (2.7→ - 3.2)	↓3	↓11	↓8	↓8	↑11	↑4	**↓26**	**↓34**
Internal capsule (9.4→ 1.1)	**↓28**	↓15	↓2	↓14	↑2	↑11	↓13	↓4
Midbrain (0.4→ - 4.4)	↑1	↓2	↓2	↓7	↓5	↑8	↓15	↓21
Motor cortex (10.4→ 4.9)	↓10	↓12	↑4	↓6	↑2	↓9	↓10	↓10
Optic tract (6.6 → 1.7)	↓10	↓7	↓14	↓14	↑1	↑5	↓12	↓11
Primary somatosensory cortex (4.9→ 4.4)	↓8	↓15	0	↓3	↑6	↓2	↓12	↓21
Putamen (8.4→ 1.4)	↓13	↓12	↓19	↓14	↑6	↑12	↓10	↓9
Somatosensory association cortex (4.1→ 1.1)	↓2	↓12	↑3	↓3	↓1	↓2	↓12	↓12
Splenium of corpus callosum (4.4→ - 3.2)	↓23	↓20	↓15	↓17	↑5	↑11	↓18	↓18
Subpial cortex (12.1→ - 8.6)	↓2	↓9	↓6	↓8	↑1	↓1	↓12	↓16
Tail of caudate nucleus (3.3→ 1.4)	↓3	↓15	**↓28**	↓15	↓1	↑19	↓15	↓27
Thalamus (3.3→ 0.7)	↓15	↓8	↑3	↓7	↑1	↑2	↓10	↓12
Visual cortex (- 6.2→ - 10.9)	↓12	↓9	↑4	↑13	↑7	↑2	↓24	**↓27**

***In vitro* assays**

Autoradiography of brain sections showed lesions (decreased tracer uptake) in regions also identified by LFB histology (Figure 4).

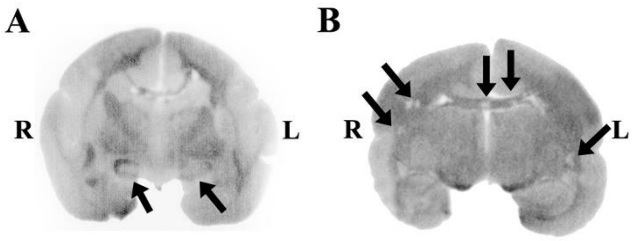

FIGURE 4. *In vitro* autoradiography illustrating demyelinated regions (arrows). A) Optic tract and B) Different regions of the corpus callosum and tail of caudate nucleus. R = right, L = left.

Differences were found between rhMOG/IFA and rhMOG/CFA brain sections stained by LFB. More lesions were found in the rhMOG/IFA group compared to rhMOG/CFA group, which presented, in general, smaller and more sparse lesions. Figure 5 illustrates some found lesions by LFB histochemistry and figure 6 shows the correlation between [^{11}C]PIB uptake and LFB histology for rhMOG/ IFA group (r^2 0.32, $P < 0.0001$) and rhMOG/CFA group (r^2 0.46, $P < 0.0001$).

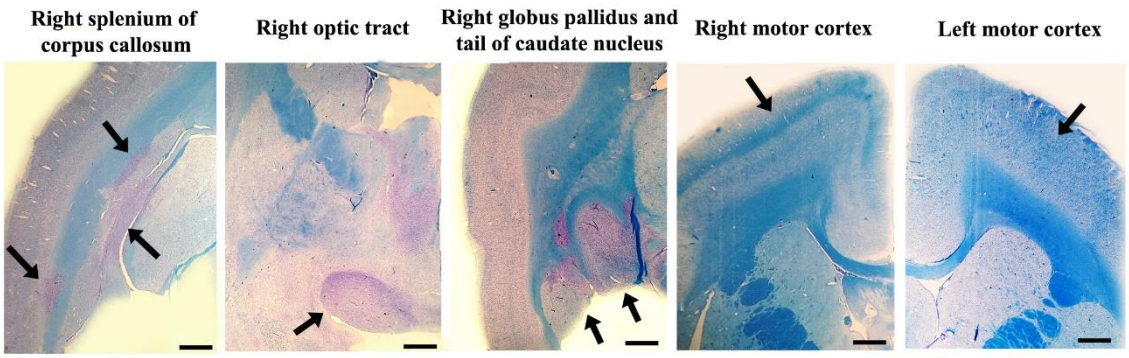

FIGURE 5. Demyelinated lesions identified by Luxol fast blue histochemistry. Arrows indicate the lesions sites. Motor cortex is represented in both hemisphere: right there is no lesion and left there is a demyelinated area. Bar size = 500 µm

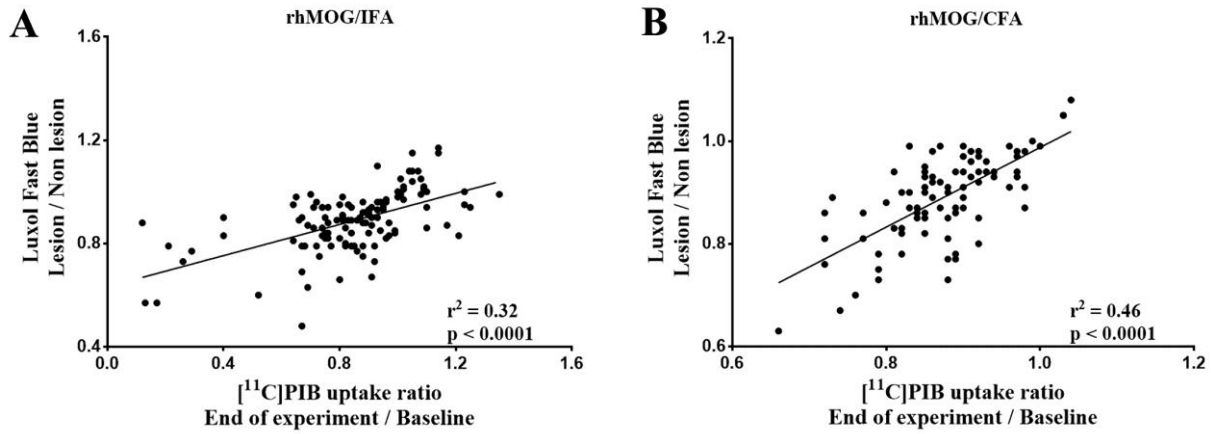

FIGURE 6. Correlation between [^{11}C]PIB uptake ratio (end of experiment/baseline) and luxol fast blue histochemistry ratio (lesion/non lesion) in the same animal and same brain region. Each dot corresponds to a brain region from an individual animal (20 to 30 samples per animal). A) rhMOG/IFA group and B) rhMOG/CFA group.

Discussion

In this study, [^{11}C]PIB PET identified demyelinated regions in different brain areas of marmoset models of progressive multiple sclerosis. Each animal presented a different disease course and lesion rate. Statically significant differences between baseline and end-of-treatment scans were observed in the cortical area of the rhMOG/CFA group, whereas significantly reduced tracer uptake was observed in white matter and grey matter regions in the rhMOG/IFA group. To our knowledge, this is the first *in vivo* PET imaging study to address demyelination detection in a non-human primate model of progressive MS, differentiating white and grey matter demyelination.

Focal demyelinated plaques are not restricted to the white matter, but are also present in the cortex and deep grey matter nuclei. In fact, cortical lesions are more abundant in the

progressive stage of MS *(20)*. However, it is difficult to identify grey matter lesions by a common clinical MRI techniques (1.5 T and 3.0 T) *(21)*. Cortical lesions are more closely correlated to cognitive impairment than white matter lesions *(22-25)* and therefore, there is a need for an *in vivo* imaging techniques that can detect and monitor these grey matter lesions.

The prof-of-concept study using [^{11}C]PIB PET in MS patients *(9)* showed that this tracer can show demyelinated lesions in RRMS patients. A comparison between different myelin PET tracers in a MS animal model *(10)* showed that [^{11}C]MeDAS performed better for myelin PET imaging then other tracers ([^{11}C]PIB and [^{11}C]CIC), however, this tracer has not been used in human so far. Since the goal of this study was to have potential translational results to MS patients, we have used [^{11}C]PIB as the myelin PET tracer. Our data complement the Stankoff et al. study *(9)* showing the potential of [^{11}C]PIB PET imaging to be used also in progressive MS.

Demyelinated lesions are predominantly present in white matter when EAE is induced by IFA, whereas grey matter demyelination is more evident when the disease is induced by CFA in the EAE marmoset model *(7)*. Our findings are in agreement with this data, since group analysis revealed statically significant reductions in [^{11}C]PIB uptake in cortical area of the animals immunized by rhMOG/CFA and more significant white matter regions in the rhMOG/IFA group, although also in some deep grey matter nuclei.

Although group significant changes in tracer uptake between baseline and end-of-treatment scans were found in some regions on a group level, there was high variability between individual animals. Disease onset, EAE score, lesion rate and localization were different in each animal, independent of immunization protocol. This fact can be explained by the outbred characteristic of the non-human primate colonies, which have the intrinsic disadvantage of higher genetic variability and thus higher variability in the results than inbred strains. On the other hand, outbred colonies have the great advantage of better mimicking the MS disease in humans *(26)*, having a higher potential for translation of the results.

Animals (M3 and M6) that presented paraplegia revealed several demyelinated regions by LFB histochemistry and a decrease in [^{11}C]PIB uptake. However, such correspondence was not found for animals M1 and M7. Although M1 and M7 presented both with monoparesis, M1 proved to have much more lesions by histology and also a stronger decrease in [^{11}C]PIB uptake than M7. This may be explained by the immunization method, as rhMOG/CFA immunization causes a more aggressive inflammatory response than rhMOG/IFA, due to the presence of a *mycobacterium* particles in the emulsion *(7)*. As a result, the high disease score of M7 may be more due to the inflammation process than demyelination.

Two animals, M5 and M8, from the rhMOG/IFA and rhMOG/CFA group respectively, presented high body weight loss, but low disease score. Both animals had only slight changes in [^{11}C]PIB uptake, which was in agreement with LFB histological findings. M8 actually showed a slight increase in [^{11}C]PIB uptake in most brain regions, with the largest increase in the head of corpus callosum (15-20%).

Animal M2 was the most interesting case. This animal had a disease score of only 0.5 due to loss of appetite, but showed a higher number of diffuse demyelinated areas in white and grey matter by LFB staining. [^{11}C]PIB uptake was strongly decreased in several brain regions (over 80% in some regions, table 1) of the right brain hemisphere. In contrast, several regions of the left brain hemisphere presented an increase in tracer uptake, suggesting some kind of compensation and/or brain plasticity.

Another theory that might explain the increased [^{11}C]PIB uptake in the left hemisphere of M2 and in most brain regions, including the corpus callosum, of M8 is the myelin basic protein (MBP) citrullination. MBP citrullination (i.e. modification of MBP protein-bound arginine to citrulline) is related to the immune response associated with myelin repair *(27)*. An increase in citrulline in the brain of MS patients compared to controls was observed by magnetic resonance spectroscopy *(28)*. If citrullination of MBP increases the [^{11}C]PIB binding affinity,

tracer uptake would be higher in newly formed myelin. However, this hypothesis needs to be further investigated.

The correlation between LBF histology and [^{11}C]PIB uptake suggests that PET imaging might be a tool for *in vivo* disease progression monitoring. It is worth to mention that the observed correlation might be underestimated due to the spatial resolution of the preclinical PET scanner (1 mm) not being able to detect too small lesions. However, the optic tract is a very small structure and the uptake differences could be detected. A strong decrease in tracer uptake in this small structure was more evident in animal M1, in which the whole optic tract was demyelinated, whereas in animals M2, M3 and M6 only part of the optic tract was demyelinated. Trying to confirm the [^{11}C]PIB specificity in this small region, we performed *in vitro* autoradiography on brain sections of the EAE marmosets. In fact autoradiography confirmed that [^{11}C]PIB uptake was decreased in the partial demyelinated optic tract, thus supporting the evidence [^{11}C]PIB could be a suitable tracer for identifying demyelination with PET.

Methodological limitations of this study has also to be mentioned: 1) Static scans and tissue to muscle ratios, rather than dynamics imaging with pharmacokinetic modeling limit the quantitative information from the images; 2) VOIs drawn in whole brain regions instead of individual lesions causes, probably, an underestimation in the reduction of tracer uptake; 3) No brain MRI of each animal is available.

Conclusion

[^{11}C]PIB PET was able to detect demyelinated lesions in grey and white matter in the EAE marmoset model. Our results warrant translation of this technique to application in humans, where it may be an useful tool for detecting demyelination in progressive multiple sclerosis, thus helping with disease progression monitoring and remyelinating therapy efficacy evaluation.

Acknowledgments

This study was supported by GE healthcare and The São Paulo Research Foundation (FAPESP - 2012/50239-6 and 2013/25049-2). EFJV received a visiting researcher fellowship from CAPES (Science Without Borders program A015_2013). Thanks also to Adilson S. Alves, Marcos Lima and Camila G Carneiro for technical assistance.

Declaration of conflicting interests

The authors declared no potential conflicts of interest with respect to the research presented in this article.

References

1. Inglese M, Bester M. Diffusion imaging in multiple sclerosis: research and clinical implications. NMR Biomed. 2010;23(7):865-72.
2. Ntranos A, Lublin F. Diagnostic Criteria, Classification and Treatment Goals in Multiple Sclerosis: The Chronicles of Time and Space. Current Neurology and Neuroscience Reports. 2016;16(10).
3. Reich DS, Lucchinetti CF, Calabresi PA. Multiple Sclerosis. New England Journal of Medicine. 2018;378(2):169-80.
4. Baker D, Amor S. Experimental autoimmune encephalomyelitis is a good model of multiple sclerosis if used wisely. Mult Scler Relat Disord. 2014;3(5):555-64.
5. Steinman L, Zamvil SS. Virtues and pitfalls of EAE for the development of therapies for multiple sclerosis. Trends Immunol. 2005;26(11):565-71.
6. t Hart BA, Gran B, Weissert R. EAE: imperfect but useful models of multiple sclerosis. Trends Mol Med. 2011;17(3):119-25.
7. t Hart BA, Dunham J, Faber BW, Laman JD, van Horssen J, Bauer J, et al. A B Cell-Driven Autoimmune Pathway Leading to Pathological Hallmarks of Progressive Multiple Sclerosis in the Marmoset Experimental Autoimmune Encephalomyelitis Model. Front Immunol. 2017;8:804.
8. Brugarolas P, Reich DS, Popko B. Detecting Demyelination by PET: The Lesion as Imaging Target. Molecular Imaging. 2018;17.
9. Stankoff B, Freeman L, Aigrot MS, Chardain A, Dolle F, Williams A, et al. Imaging central nervous system myelin by positron emission tomography in multiple sclerosis using [methyl-(1)(1)C]-2-(4'-methylaminophenyl)- 6-hydroxybenzothiazole. Ann Neurol. 2011;69(4):673-80.
10. Faria Dde P, Copray S, Sijbesma JW, Willemsen AT, Buchpiguel CA, Dierckx RA, et al. PET imaging of focal demyelination and remyelination in a rat model of multiple sclerosis: comparison of [11C]MeDAS, [11C]CIC and [11C]PIB. Eur J Nucl Med Mol Imaging. 2014;41(5):995-1003.
11. Yang FY, Lu WW, Lin WT, Chang CW, Huang SL. Enhancement of Neurotrophic Factors in Astrocyte for Neuroprotective Effects in Brain Disorders Using Low-intensity Pulsed Ultrasound Stimulation. Brain Stimul. 2015;8(3):465-73.
12. Huang SL, Chang CW, Lee YH, Yang FY. Protective Effect of Low-Intensity Pulsed Ultrasound on Memory Impairment and Brain Damage in a Rat Model of Vascular Dementia. Radiology. 2017;282(1):113-22.

13. Fodero-Tavoletti MT, Rowe CC, McLean CA, Leone L, Li QX, Masters CL, et al. Characterization of PiB binding to white matter in Alzheimer disease and other dementias. J Nucl Med. 2009;50(2):198-204.
14. Jagessar SA, Heijmans N, Oh L, Bauer J, Blezer EL, Laman JD, et al. Antibodies against human BLyS and APRIL attenuate EAE development in marmoset monkeys. J Neuroimmune Pharmacol. 2012;7(3):557-70.
15. Jagessar SA, Heijmans N, Blezer EL, Bauer J, Weissert R, t Hart BA. Immune profile of an atypical EAE model in marmoset monkeys immunized with recombinant human myelin oligodendrocyte glycoprotein in incomplete Freund's adjuvant. J Neuroinflammation. 2015;12:169.
16. Yuasa S, Nakamura K, Kohsaka S. Stereotaxic Atlas of the Marmoset Brain

With Immunohistochemical Architecture and MR Images. Tokyo, Japan: National Institute of Neuroscience (JP); 2010 March, 2010.
17. Le Foll B, Chefer SI, Kimes AS, Shumway D, Goldberg SR, Stein EA, et al. Validation of an extracerebral reference region approach for the quantification of brain nicotinic acetylcholine receptors in squirrel monkeys with PET and 2-F-18-fluoro-A-85380. Journal of Nuclear Medicine. 2007;48(9):1492-500.
18. Faria DdP, de Vries EFJ, Sijbesma JWA, Buchpiguel CA, Dierckx RAJO, Copray SCVM. PET imaging of glucose metabolism, neuroinflammation and demyelination in the lysolecithin rat model for multiple sclerosis. Multiple Sclerosis Journal. 2014;20(11):1443-52.
19. Faria DdP, de Vries EFJ, Sijbesma JWA, Dierckx RAJO, Buchpiguel CA, Copray S. PET imaging of demyelination and remyelination in the cuprizone mouse model for multiple sclerosis: A comparison between [C-11]CIC and [C-11]MeDAS. Neuroimage. 2014;87:395-402.
20. Lassmann H, van Horssen J, Mahad D. Progressive multiple sclerosis: pathology and pathogenesis. Nature Reviews Neurology. 2012;8(11):647-56.
21. Kangarlu A, Bourekas EC, Ray-Chaudhury A, Rammohan KW. Cerebral cortical lesions in multiple sclerosis detected by MR imaging at 8 Tesla. American Journal of Neuroradiology. 2007;28(2):262-6.
22. Amato MP, Portaccio E, Goretti B, Zipoli V, Battaglini M, Bartolozzi ML, et al. Association of neocortical volume changes with cognitive deterioration in relapsing-remitting multiple sclerosis. Archives of Neurology. 2007;64(8):1157-61.
23. Amato MP, Bartolozzi ML, Zipoli V, Portaccio E, Mortilla M, Guidi L, et al. Neocortical volume decrease in relapsing-remitting MS patients with mild cognitive impairment. Neurology. 2004;63(1):89-93.
24. Portaccio E, Amato MP, Bartolozzi ML, Zipoli V, Mortilla M, Guidi L, et al. Neocortical volume decrease in relapsing-remitting multiple sclerosis with mild cognitive impairment. Journal of the Neurological Sciences. 2006;245(1-2):195-9.
25. Kalinowska-Lyszczarz A, Pawlak MA, Pietrzak A, Pawlak-Bus K, Leszczynski P, Puszczewicz M, et al. Subcortical gray matter atrophy is associated with cognitive deficit in multiple sclerosis but not in systemic lupus erythematosus patients. Lupus. 2018;27(4):610-20.
26. t'Hart BA, van Meurs M, Brok HPM, Massacesi L, Bauer J, Boon L, et al. A new primate model for multiple sclerosis in the common marmoset. Immunology Today. 2000;21(6):290-7.
27. Yang L, Tan DW, Piao H. Myelin Basic Protein Citrullination in Multiple Sclerosis: A Potential Therapeutic Target for the Pathology. Neurochemical Research. 2016;41(8):1845-56.
28. Oguz KK KA, Aksu AO , Karabulut E , Serdaroglu A , Teber S , Haspolat S , Senbil N , Kurul S , Anlar B. Assessment of citrullinated myelin by 1H-MR spectroscopy in early-onset multiple sclerosis. AJNR Am J Neuroradiol. 2009;30(4):6.